



## RESEARCH LETTER

10.1029/2019GL082362

## Informing Future Risks of Record-Level Rainfall in the United States

## Key Points:

- Spatial clustering can be used to create stable projections of extreme precipitation events
- Analysis over the United States suggests 1,000-year events will be up to 5 times more frequent under 2 degree C warming
- Differences in projections between regions are evident, with the U.S. East Coast and mountain regions showing large intensification

## Supporting Information:

- Supporting Information S1

## Correspondence to:

B. M. Sanderson,  
sanderson@cerfacs.fr

## Citation:

Sanderson, B. M., Wobus, C., Mills, D., Zarakas, C., Crimmins, A., Sarofim, M. C., & Weaver, C. (2019). Informing future risks of record-level rainfall in the United States. *Geophysical Research Letters*, 46, 3963–3972. <https://doi.org/10.1029/2019GL082362>

Received 6 NOV 2018

Accepted 26 MAR 2019

Accepted article online 1 APR 2019

Published online 10 APR 2019

©2019. The Authors.

This is an open access article under the terms of the Creative Commons Attribution-NonCommercial-NoDerivs License, which permits use and distribution in any medium, provided the original work is properly cited, the use is non-commercial and no modifications or adaptations are made.

Benjamin M. Sanderson<sup>1</sup> , Cameron Wobus<sup>2</sup> , Dave Mills<sup>3</sup> , Claire Zarakas<sup>3,4</sup>, Allison Crimmins<sup>5</sup> , Marcus C. Sarofim<sup>5</sup> , and Chris Weaver<sup>5</sup>

<sup>1</sup>CERFACS, Toulouse, France, <sup>2</sup>Lynker Technologies, Boulder, CO, USA, <sup>3</sup>Abt Associates, Boulder, CO, USA,

<sup>4</sup>Department of Atmospheric Science, University of Washington, Seattle, WA, USA, <sup>5</sup>United States Environmental Protection Agency, Washington, DC, USA

**Abstract** The changing risk of extreme precipitation is difficult to project. Events are rare by definition, and return periods of heavy precipitation events are often calculated assuming a stationary climate. Furthermore, ensembles of climate model projections are not large enough to fully categorize the tails of the distribution. To address this, we cluster the contiguous United States into self-similar hydroclimates to estimate changes in the expected frequency of extremely rare events under scenarios of global mean temperature change. We find that, although there is some regional variation, record events are projected in general to become more intense, with 500-year events intensifying by 10–50% under 2 °C of warming and by 40–100% under 4 °C of warming. This analysis could provide information to inform regional prioritization of resources to improve the resilience of U.S. infrastructure.

## 1. Introduction

Flooding associated with extreme rainfall represents one of the deadliest and most costly types of natural disaster worldwide, severely affecting developing and developed countries alike (Munich, 2015). For example, according to a recent UN report, flooding accounted for nearly half of all weather-related disasters from 1995–2015, affecting 2.3 billion people (Wahlstrom & Guha-Sapir, 2015). In the United States, 90% of all federally declared natural disasters involve flooding (FEMA, 2015). Increases in the frequency and severity of extreme precipitation due to climate change therefore pose substantial risks to future life and property (Wobus et al., 2017).

Governments, institutions, and communities manage the risks associated with extreme precipitation by establishing design and performance standards for buildings, dams, levees, and other infrastructure, as well as by placing restrictions on where and how development can take place (Crichton, 2008; Kundzewicz & Takeuchi, 1999; Tollan, 2002). These standards and guidelines are built, however, entirely on observations of the historical past, and therefore if the frequency and magnitude of extreme precipitation events change, these standards could lead to inadequate preparation for future risks (Herring et al., 2015; Maxwell et al., 2018; Wobus et al., 2017).

Currently, climate models are the main tool the scientific community uses to make projections of future climatic conditions under changing boundary conditions. But assessing extreme precipitation risk from the presently available archive of climate simulations is nontrivial. Basic theory has long predicted (Trenberth et al., 2003) that the most extreme precipitation events are governed by simple thermodynamic principles: Warmer air is capable of holding more moisture, and thus events which significantly deplete the atmospheric column of moisture will become, on average, more extreme in a warmer climate. However, when aggregated globally, the range of models available in the Coupled Model Intercomparison Project, version 5 (CMIP5; Taylor et al., 2012) encompasses a variety of responses of extreme precipitation to warming, due in part to differences in the parameterizations in convection and microphysical processes (Singh & O’Gorman, 2014). As such, a single model is unable to capture the diversity of possible changes in future behavior and thus any comprehensive risk analysis requires an ensemble approach.

In general, projections of extreme precipitation events are made for relatively short return periods in models (e.g., 20 years as in Wuebbles et al., 2014) and observations (20-year events in Kunkel et al., 2003, and 100 years in Mishra & Singh, 2010). However, without very large ensemble sizes such as Kay et al. (2015),

there are not enough simulated years to directly estimate extreme value characteristics at some longer, policy-relevant return intervals (such as 1,000-year or probable maximum precipitation, which are used for design standards for dams, for example).

The sampling issue has been addressed in a number of ways, a common approach being spatial aggregation. When aggregated at a global (Pendergrass et al., 2015) or continental (Fischer et al., 2013) level, precipitation distributions are well enough sampled in the tail to resolve the changing nature of extreme precipitation in a future scenario. However, while such scales can be informative for understanding the general characteristics of rainfall in different models or for global scale attribution statements, they are not directly useful for planning and adaptation at a regional or subnational scale. Furthermore, the physical interpretation of such distributions is complicated by the fact that large regions cover a wide range of precipitation regimes, and so the events represented are not drawn from a single distribution.

An alternative and potentially simpler approach to resolving the sampling issue is to use spatial clustering to identify regions which broadly share precipitation characteristics, such that precipitation events within a cluster can be approximated to be drawn from the same distribution (Gong & Richman, 1995; Hargrove & Luxmoore, 1998; Yavuz & Erdoğan, 2012; Zhang et al., 2001). These approaches have had some qualitative success in identifying self-similar precipitation regimes within a wider domain. There have also been efforts to combine extreme value parameters and traditional k-means clustering to produce regions of comparable extreme precipitation behaviour (Bernard et al., 2013; Carreau et al., 2016).

In this study, we build on such approaches and use spatially clustered precipitation data to provide information on changing risk of extreme precipitation on a more useful scale for regional risk analysis and adaptation. Using this spatial clustering approach, we seek to characterize the magnitude of extremely rare (1 in 1000 years) historical precipitation events in each of 15 regions in the continental United States, as well as the changing probability of those events under a range of warming scenarios.

This study supports increasing calls to reframe climate change assessment to better aid in real-world risk management, incorporating principles and techniques from the public safety and financial risk fields (Kennel et al., 2016; King et al., 2015; Kunreuther et al., 2013; National Academies of Sciences, Engineering, and Medicine, 2016; Weaver et al., 2017). These calls highlight requests for better information on how low-probability, high-consequence extremes are changing and how the statistics of localized events vary as a function of global-mean temperature increase. Quantifying such risk-relevant metrics is challenging and often subject to limitations in data availability. This study is a first step in advancing this endeavour by proposing an approach for estimating changes in extreme precipitation at a regional scale using existing data.

## 2. Materials and Methods

### 2.1. Clustering Regions Based on Precipitation Characteristics

Our goal is to boost the sample of annual maximum precipitation values to increase confidence in the estimates of events of up to 1,000-year return values. In order to be able to make any such statement, a comparable number of sample years must be considered. We thus propose a novel spatial clustering algorithm which uses a traditional interpoint distance metric (Singh et al., 2013) but ensures each cluster has greater than or equal to a specified number of elements. As well as the extreme precipitation characteristics, we also seek to consider sites which have similar general precipitation characteristics to increase the confidence that extreme precipitation events within each cluster represent similar processes. Hence, we also incorporate a measure of physical distance, fraction of dry days, and mean precipitation into the distance metric. It was found in the development of the algorithm that this additional information helped to distinguish between regions where maximum precipitation events are associated, for example, with intense convective storms (as in the U.S. Mountain West) or with large scale synoptic events (as in the Pacific Northwest). Using only the information about extreme events was found to produce less coherently clustered regions (see supporting information).

### 2.2. Defining an Interpoint Distance Metric

The code for the approach is supplied with the paper. The clustering algorithm requires an input of a matrix of interpoint distances. How these distances are defined is fundamentally subjective, but for our application we are primarily concerned with choosing points whose precipitation values are drawn from similar distributions.

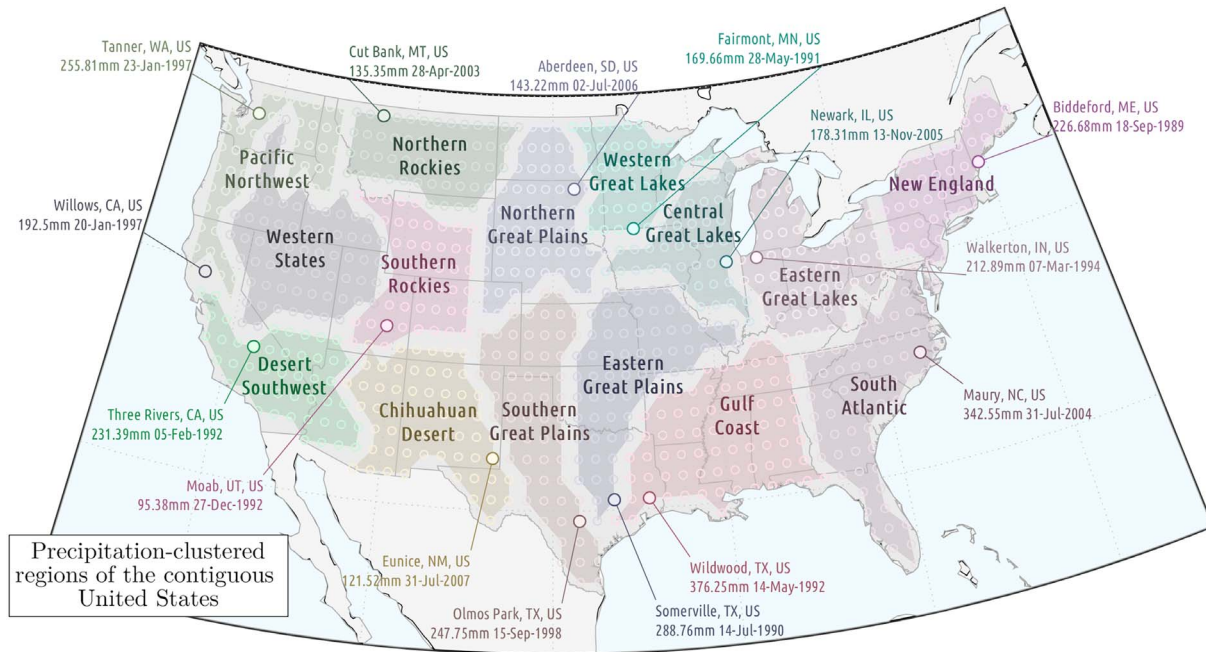


**Figure 1.** An illustration of the regional clusters used for the analysis. Each point represents a single grid cell or cluster element, and points of the same color are in the same cluster. The location of the most extreme event in the historical time series in the cluster is highlighted in each case (and detailed in supporting information Table S1). The date listed is the first date of the 3 days described in the event, and the rainfall amount is the grid cell average Global Precipitation Climatology Centre precipitation accumulation during the 3-day period. Each cluster is ascribed a verbal description for clarity.

An interpoint distance metric is computed using information derived from the distribution of daily precipitation at the point level in the Global Precipitation Climatology Centre (GPCC) 1° reanalysis product (Becker et al., 2013). The algorithm is designed such that each cluster has at least 40 points, a number which was found to be large enough to result in relatively stable extreme value parameter fits: given 26 years of data in the GPCC data set, this ensures that each cluster has at least 1,040 years of grid point data (other population sizes are tested in the supporting information). Figure 1 shows the resulting precipitation clusters. As expected, geographical features (e.g., mountain/desert regions) provide notable boundaries between clusters.

For each grid point, a vector is compiled using seasonal information on the median and 99th percentile of precipitation, along with the seasonal fraction of dry days. This information is combined with a physical interpoint distance metric to establish point-wise similarities between each one of the grid points in the domain. We use this matrix as an input for the clustering algorithm, the results of which are illustrated in Figure 1.

The variables used in the distance metric are illustrated in supporting information Table S2. The distance ( $D_0$ ) combines a number of components:

$$D_0(i, j) = r \cos^{-1} (\cos \theta_i \cos \theta_j + \sin \theta_i \sin \theta_j \cos (\varphi_i - \varphi_j)), \quad (1)$$

where  $r$  is the Earth's radius in kilometers, and  $\theta_{i,j}$  and  $\varphi_{i,j}$  are the latitudes and longitudes of points  $i$  and  $j$  respectively.

The distance metric corresponding to fraction of dry days ( $D_1$ ) is calculated as follows:

$$D_1(i, j) = \sum_s (F^{dry}(i, s) - F^{dry}(j, s))^2, \quad (2)$$

where  $s$  is the season and  $(i, j)$  are the two grid cells being compared.

The distance metric corresponding to the 50th percentile of rainy day seasonal precipitation ( $D_2$ ) is calculated as follows:

$$D_2(i, j) = \sum_s (P_{50}^{wet}(i, s) - P_{50}^{wet}(j, s))^2. \quad (3)$$

Finally, the distance metric corresponding to the 99th percentile of rainy day seasonal precipitation ( $D_3$ ) is calculated as follows:

$$D_3(i, j) = \sum_s (P_{99}^{\text{wet}}(i, s) - P_{99}^{\text{wet}}(j, s))^2. \quad (4)$$

Each distance type  $D_x$  is then normalized to form a unitless distance metric  $\delta_x$ . We normalize each distance metric over the contiguous United States domain, such that

$$\delta_x(i, j) = D_x(i, j) \sum_{i \neq j} \frac{n_i^2}{D_x(i, j)}, \quad (5)$$

where  $n_i$  is the total number of grid cells in the U.S. domain.

We then combine the various elements of the distance metric into a single measure:

$$\delta(i, j) = \alpha \delta_0(i, j) + \delta_1(i, j) + \delta_2(i, j) + \delta_3(i, j), \quad (6)$$

where  $\alpha$  is a parameter to modulate the weight of the physical distance metric relative to the precipitation characteristic metrics. We choose a value of  $\alpha = 9$  for this study—which was found empirically to preserve features associated with known precipitation regimes while also maintaining coherent and localized spatial structures.

### 2.3. Population Clustering

We propose an algorithm which separates the domain into approximately equally sized subdomains while sharing common bulk precipitation characteristics. Traditional k-means clustering performs only the latter; hence, we propose an iterative algorithm to address both issues. The code for the algorithm is provided, but the process is as follows.

1. Allocate an initial parameter:  $n_c$ , the desired number of clusters.
2. Initially allocate one cluster to each element in the domain, forming  $n$  clusters in total (where  $n$  is initially  $n_i$ , the total number of grid cells).

Then perform the following loop, while there exists a greater number of clusters than  $n_c$ :

1. For each of the clusters  $n$ , find the representative element in the entire domain which has the smallest average distance to the elements in  $n$ .
2. Using the representative elements as approximate centroids, construct an approximate intercluster distance metric  $\Delta$ .
3. Of the total  $n$  clusters, then find the subset of clusters  $s$  which each has the smallest number of elements (this will be 1, initially).
4. Use the intercluster distance matrix  $\Delta$  to determine the member of  $s$  which is closest to one of the other cluster centroids in the set of  $n$ . This cluster,  $n_x$  will be eliminated from the set.
5. Loop through the elements of  $n_x$ , and for each element, determine the closest centroid within the remaining clusters.
6. Form a new set of  $n - 1$  clusters, without the  $n_x$  cluster, where all elements of  $n_x$  are individually reallocated to the appropriate remaining clusters.

For the purposes of this study, a value of  $n_c = 15$  was chosen to produce solutions which provided sufficient points to resolve the tails of the aggregated precipitation distributions, while maintaining a diversity of precipitation regimes. In the main analysis used in this paper, the minimum number of elements in any cluster,  $s_{\min}$  is 40.

#### 2.3.1. Data Preparation

We focus here on 3-day events as a proxy for potential flood risk (Kunkel et al., 1999; Pielke & Downton, 2000). We find the most extreme 3-day rainfall event in each cluster over the entire time-span of the data set. The 3-day accumulated GPCP grid cell average precipitation associated with each of these events (each a record in its local region during the observed period) are listed in supporting information Table S1. The  $1^\circ$  resolution (also typical of the CMIP5 models) represents a scale of roughly 100 km within the contiguous United States, though clearly there may be significant heterogeneity at finer scale. As such, it is expected that rain gauge precipitation records may be substantially greater than those in supporting information Table S1.

Many of these record events caused significant damage and drew extensive coverage in popular media, news reports, and government publications. These observations place each cluster's most extreme event into a societally relevant context. For example, the 1994 flood event in the Gulf Coast cluster (o) in Southeast Texas required 54 million U.S. dollars in Federal disaster assistance and resulted in private insurance losses of 700 million dollars (Liscum & East, 1995). The 1999 event in the South Atlantic cluster (n) in North Carolina was associated with hurricane Floyd, which resulted in 56 deaths (Rappaport, 2000) and 6 billion dollars in losses (Bin & Polasky, 2004). The 2006 event (c) in Moab UT caused extensive damage to National Park infrastructure (National Park Service news release, October 10, 2006, n.d)

We use the CMIP5 ensemble to consider the changing likelihood of events such as those in supporting information Table S1 both in the present day as well as at higher global mean warming thresholds of 1.5, 2, 3, and 4 °C above preindustrial levels (see supporting information Table S5). The present day is represented in each model by the 26-year period which first exhibits an average 0.67 °C warming above preindustrial levels, corresponding to the observed warming during the period 1988–2013 relative to a preindustrial baseline in HadCRUT (Morice et al., 2012). We use the historical and RCP8.5 simulations to represent simulated climate at different warming thresholds (RCP8.5 is a Representative Concentration Pathway describing a high greenhouse gas emission future; Riahi et al., 2011).

We consider each member of the CMIP5 ensemble to be an equally likely projection of the future (as concluded to be appropriate in Knutti et al., 2010). Despite some proposed analysis schemes to account for model skill or interdependency (Abramowitz & Bishop, 2015; Herger et al., 2017; Sanderson et al., 2017), there is no consensus on the best approach or strong evidence to date that such approaches can significantly improve projection accuracy relative to model democracy (Wuebbles et al., 2017).

#### 2.4. Extreme Value Analysis

An extreme value distribution is estimated from the GPCC data for each grid point for the entire historical period 1988–2013, and a generalized extreme value distribution (GEV) fit to the set of maximum values in the cluster provides an estimate of the return period associated with each maximum observed rainfall event. We determine the annual maximum 3-day precipitation value between 1988 and 2013 for each grid cell in the GPCC data set for each point in the contiguous United States (note that although NOAA publishes return frequency estimates for the United States (Bonnin et al., 2006), we compute our own here to provide comparable estimates to the model output).

The data set is at 1° resolution, with 834 points in total in the entire domain. For each cluster  $n_i$ , all points are combined to form a vector  $X_i$  of block maximum 3-day precipitation values, assumed to be independently sampled (we test this later), such that each distribution has at least  $s_{\min} * 26$  points (given 26 years in the sample). The maximum event  $M_i = \max(X_i)$  in the entire distribution is recorded, and the  $X_i$  vector is used to fit a GEV,  $F_i(p)$ , where  $p$  represents 3-day annual maximum precipitation.

A separate GEV distribution of maximum 3-day precipitation values is constructed for each CMIP5 model, warming level, and cluster region. The fit can be used to estimate the precipitation value which would correspond to a 100- or 1,000-year event in the region during the reference or baseline period in each model. The baseline period is chosen such that global mean warming is 0.67 °C above the 1851–1880 period, corresponding to the warming seen in HadCRUT in the years 1988–2013.

For each model, the first ensemble member of RCP8.5 has been used to represent warmer climates. The time period corresponding to the GPCC data set is 1988–2013, during which time the globally averaged warming in HadCRUT (Morice et al., 2012) is 0.67 °C above 1851–1880 levels. Correspondingly, we select the 26-year period where the model global moving average warming is  $t = 0.67$  °C above 1851–1880 levels. Similarly, we consider warming thresholds for 40-year periods in which future climate first exceeds  $t = 1.5, 2, 3,$  and 4 °C of warming above 1851–1880 values.

For each model considered, precipitation data are linearly interpolated to the GPCC grid, and points are allocated to the observationally derived clusters  $n$ . For each model  $m$ , warming level  $t$ , and cluster  $i$ , we construct a block maximum distribution using the 3-day maximum precipitation which occurred in model  $m$  in each grid cell of cluster  $i$  in each year of the 26-year window used to represent warming level  $t$ . We call this vector  $Y_i^{t,m}$  and fit a GEV distribution  $G_i^{t,m}(p)$ .

Given the actual historical precipitation record  $p_i^{\max}$  in cluster  $i$ , we then can produce a corresponding percentile-mapped value in each model  $m$  for the reference time period. The percentile-mapped values for

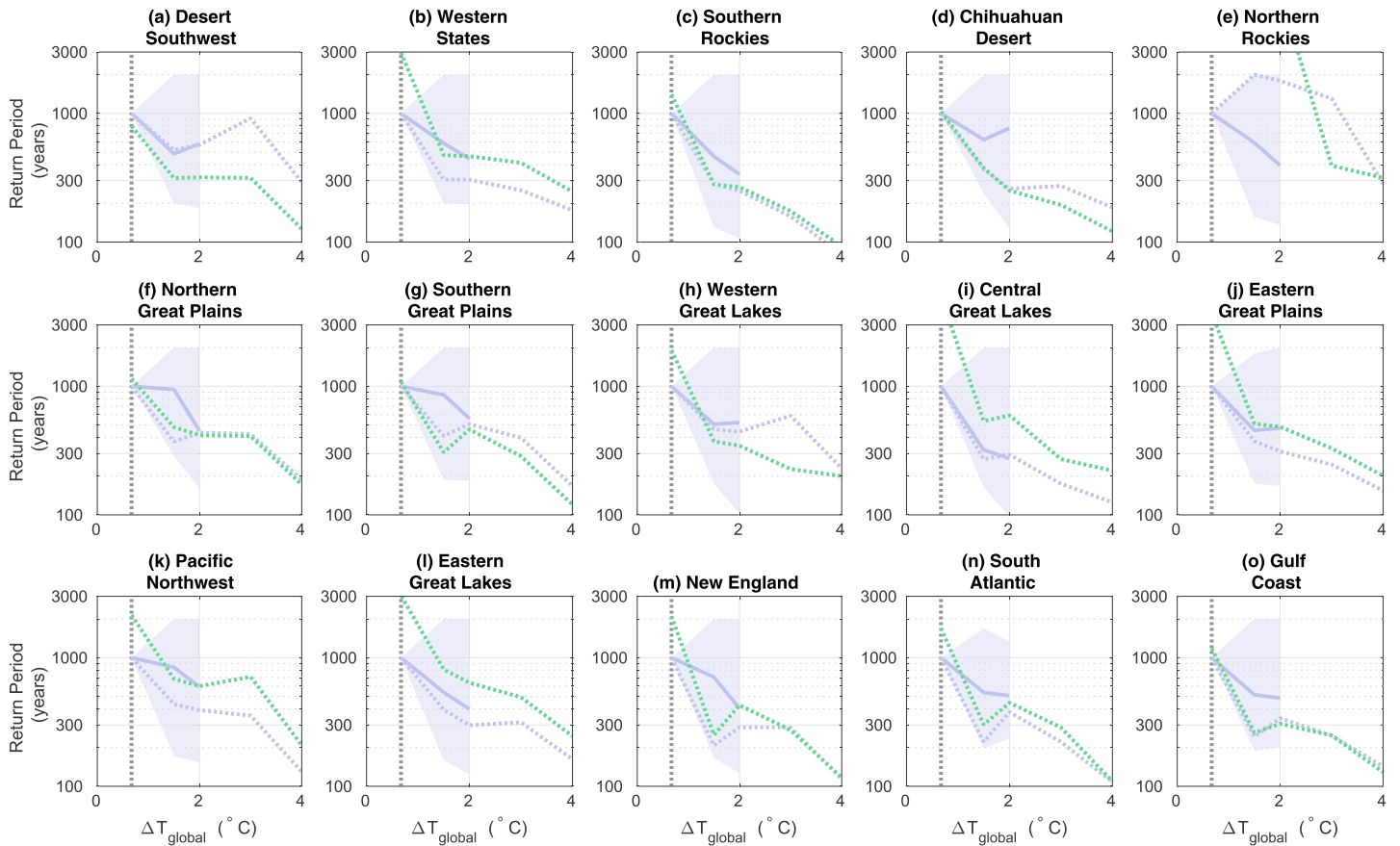


**Figure 2.** The changing return periods of precipitation events as a function of global mean temperature, where each subplot represents a specific regional cluster. In each plot, present-day (2013–2017) global mean warming levels relative to 1851–1880 are illustrated by the vertical dotted line. Purple elements (solid and dotted lines and the shaded region) correspond to the frequency of a precipitation event equal in magnitude to a 1,000-year precipitation event in the present day, while green elements correspond to the future frequency of an event equal in magnitude to the historical record extreme event for the cluster. Solid lines are the median future frequency for the available CMIP5 ensemble at a given temperature, and the shaded area spans the 10th to 90th percentiles of the distribution. The dotted lines (green and purple) correspond to the median of the subset of CMIP5 models which reach  $T_g = 4^\circ$  at some point during the simulation. Subplots (a)–(o) correspond to regions illustrated in Figure 1. CMIP5 = Coupled Model Intercomparison Project, version 5.

precipitation records in the model reference period are then derived using  $F_i(p)$  and  $G_i^{1,m}(p)$ , such that

$$P_i^{\max,m} = G_i^{1,m}(F'_i M_i), \quad (7)$$

where  $F'_i$  is the inverse Cumulative Distribution Function of  $F_i(p)$ . Similarly, we can compute the future return period of a present-day 1,000-year event in model  $m$  and cluster  $i$  as follows:

$$\left(1 - G_i^{t,m}(G_i^{1,m}(1 - 1/1,000))\right)^{-1} \quad (8)$$

In order to predict the future intensity of an event with a specific return period in the future, we combine a simulated present day precipitation distribution with a percentile change due to warming derived from the model  $m$ :

$$S_i^{t,m} = F_i(p) + (G_i^{t,m}(p) - G_i^{1,m}(p)), \quad (9)$$

where  $p$  is the percentile of the event in the distribution, equivalent to  $(1 - T)^{-1}$  for a return period  $T$ .

In Figure 4, we produce estimates for precipitation values associated with a given return period for a given temperature level  $t$  and cluster  $i$  by taking the mean of all models  $m$  which sample up to  $T_g = 4^\circ\text{C}$  (starred in supporting information Table S5).

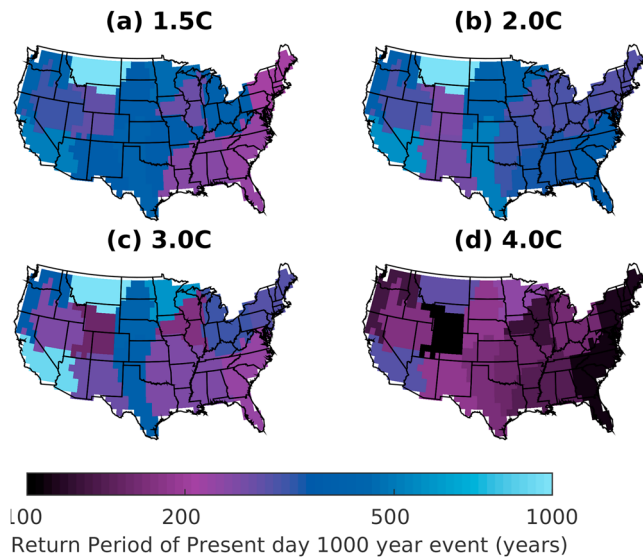


**Figure 3.** An illustration of the changing return periods, by region, of what would have been a 1,000-year event during the Global Precipitation Climatology Centre data set period 1988–2013. The color in each cluster corresponds to the median of models reaching  $T_g = 4^\circ\text{C}$  during the simulation. The colors correspond to the purple dotted line in Figure 2, and the data are tabulated in supporting information Table S3. Subplots (a)–(d) correspond to changes predicted at 1.5C, 2C, 3C, and 4C of global mean warming, respectively.

100- and 500-year events). We find that in all clusters, 500-year events will become more intense in a warmer world, but some clusters show more dramatic results than others. Clusters on the U.S. East Coast show a more than doubling of the intensity of a 500-year event, whereas the western states cluster, for example, shows less of a dramatic change in the intensity of 500-year events.

The comparison of comparable historical 100- and 500-year return values from GPCC with the modeled results also indicates that model precipitation in some regions is underrepresenting or overrepresenting present-day extremes. Models underestimate historical extremes in the clusters strongly affected by tropical cyclones (South Atlantic and Gulf Coast clusters) and overestimate in mountain regions (Southern Rockies, Chihuahuan Desert, and western states). In each case, the models are not well representing the processes generally associated with the most extreme rainfall levels.

### 3.1.2. Sensitivity Analyses

We consider three degrees of freedom in the clustering approach and how they influence our results. In the first case, we consider how modifying the desired number of clusters changes the distribution of regions. Supporting information Figure S1 illustrates that varying  $n_c$  produces the desired effect of splitting the domain into broadly equally sized regions, with borders separating different climatological regimes. This analysis, as for the main analysis in the paper, uses distance weights which combine mean precipitation, fraction of dry days and the 95th percentile of precipitation.

To understand how the distribution would change if only the 95th percentile was used, we repeat the clustering process for 15 clusters, using both the full climatological vector (as in the main paper) and only the extreme information (supporting information Figure S2). We find that in the latter case, regions are more spread out across the domain, spanning regions where the extreme precipitation events are likely to be associated with different types of physical phenomena.

Finally, the parameter  $\alpha$  allows us to further coagulate regions to be more spatially contained within the larger domain. The effect of this parameter is illustrated in supporting information Figure S3, which shows that a variation in  $\alpha$  over 2 orders of magnitude can result in regions which are either compact (for large values of  $\alpha$ ) or with more complex borders following climatological boundaries (at small values of  $\alpha$ ). Choosing a nonzero value of  $\alpha$  allows the method to produce regions for communication which are a trade-off between climatological consistency and spatial coherency.

For a given return period, we use the fitted GEVs to assess what the precipitation intensity would be both for the reference time period and the chosen future time period. The difference between these values indicates the expected intensification at that return period. An extreme value distribution fitted to the GPCC data yields the expected observed historical precipitation level for a given return period. Finally, this observational value is added to the expected intensification to yield an estimate for future precipitation magnitude at different warming levels.

## 3. Results

### 3.1. Future Projections of Extreme Precipitation

#### 3.1.1. Extreme Value Analysis

Figure 2 shows the results of an extreme value analysis used to project the frequency of historical 1,000-year events at greater levels of warming in each cluster.

The results suggest that historical 1,000-year events will occur 2–5 times more frequently under 2 °C warming (depending on the region). Under 4 °C of warming (for those models which reach that level under RCP8.5), a present-day 1,000-year event is projected to be 5–10 times more frequent. The greatest increase in frequency is seen in the U.S. East Coast, the Southern Great Plains, and southern Rocky Mountain clusters (illustrated on a map of the continental United States in Figure 3).

We can also use this analysis to consider the expected intensity of the most extreme events which might be experienced in the future (Figure 4, for

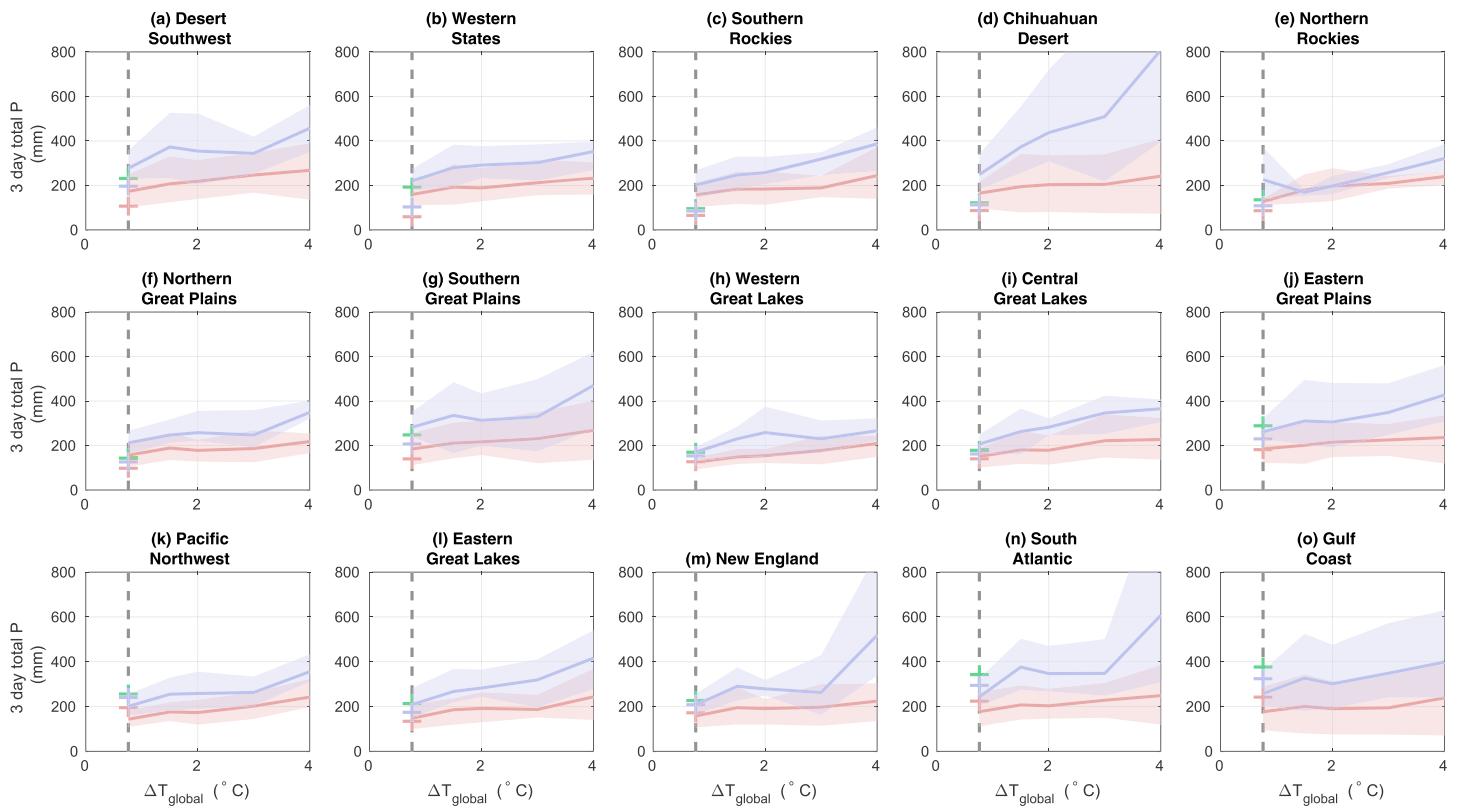


**Figure 4.** The predicted intensity of extreme precipitation in various regions of the contiguous United States as a function of global mean temperature. The vertical axis in each case represents 3-day annual maximum precipitation. Solid red and blue lines show expected 100- and 500-year events, respectively, while shaded areas indicate the lower and upper bounds of the subset of models which reach  $4^{\circ}\text{C}$  of warming. Red and blue crosses show comparable 100- and 500-year historical return periods as computed by the historical generalized extreme value fit. The green cross shows, for reference, the intensity of the record observed event for the cluster. The vertical dotted black line shows the average warming in 2013–2017 as assessed from HadCRUT. Data for this plot are tabulated in supporting information Table S4. Subplots (a)–(o) correspond to regions illustrated in Figure 1.

### 3.1.3. Model Subsetting for Higher Warming Levels

Only a subset of the models considered here reaches  $4^{\circ}\text{C}$  of warming above preindustrial levels during their RCP8.5 simulation. As such, results relating to 3 and  $4^{\circ}\text{C}$  of warming use only a subset of four models (those starred in supporting information Table S5) to represent return period estimates. One can assess the expected influence of using only four models for the higher temperature thresholds in Figure 2 for global mean temperatures of  $2^{\circ}\text{C}$  or less where all the models are available. Based on this comparison, the smaller set is found to broadly replicate the mean trend in most regions. This smaller set cannot represent the uncertainty in the full CMIP5 estimate, so we report only the mean value for warming values of greater than  $2^{\circ}\text{C}$  without showing their associated uncertainties.

## 4. Conclusions

Advances in climate science made in previous decades have enabled the community to make confident statements that the planet is warming (Gleckler et al., 2012; Wuebbles et al., 2017) and that this warming has had a detectable influence on the frequency (Fischer & Knutti, 2014; Min et al., 2011) and intensity of extreme precipitation (Wuebbles et al., 2014). However, there is a scarcity of information on the future evolution of the types of extreme precipitation events that would exceed the tolerances of today's infrastructure. Such information is necessary to inform policy makers, urban planners, and regional governing bodies when making decisions with the potential to avoid significant loss of life, property, or livelihood. As such, producing useful projections of exactly what individual communities should expect under climate change is an enduring challenge.

This study takes a step toward this goal by improving characterization of the risk of extreme precipitation. We outline a potential methodology for providing information on multicentury precipitation events at a

regional scale. We present this approach as a proof of concept, given that there are uncertainties associated with free parameters in the approach relating to cluster size, cohesion, distance metrics, and assumed extreme value distribution. A formal risk assessment would require the effects of these parameters to be more comprehensively sampled and understood.

While this analysis offers a useful methodology for extracting information on changes in extreme precipitation events from existing data, important questions about the direct usability of these regional projections, in planning and decision-making contexts, remain. For example, city-level accumulation might be significantly greater than the average of the 100-km grid cell in which the city is located, and because there is a relatively small set of models in the archive (especially at high warming levels), our results are not a comprehensive sample of all possible future behavior. In some regions, model results might be biased because we know that some physical processes relevant to extreme precipitation are not represented in the CMIP5 models, such as tropical cyclones on the U.S. Gulf Coast. Nevertheless, there is value in operational use of analytic approaches that can at least bound the problem, delineating a planning envelope for risk assessment and providing plausible futures against which to stress test valued assets (Stern, 2013).

### Acknowledgments

The views expressed in this document are those of the authors and do not necessarily reflect those of their affiliated institutions including the U.S. Environmental Protection Agency. This research was funded by the U.S. Environmental Protection Agency under contract EPBPA16H0003. Benjamin Sanderson is supported by the French National Research Agency, project ANR-17-MPGA-0016. Complete code to reproduce this study is provided at this repository: <https://data.mendeley.com/datasets/v6ztmhd93c/1>.

### References

- Abramowitz, G., & Bishop, C. H. (2015). Climate model dependence and the ensemble dependence transformation of CMIP projections. *Journal of Climate*, *28*(6), 2332–2348.
- Becker, A., Finger, P., Meyer-Christoffer, A., Rudolf, B., Schamm, K., Schneider, U., & Ziese, M. (2013). A description of the global land-surface precipitation data products of the Global Precipitation Climatology Centre with sample applications including centennial (trend) analysis from 1901 to present. *Earth System Science Data*, *5*(1), 71–99. <https://doi.org/10.5194/essd-5-71-2013>
- Bernard, E., Naveau, P., Vrac, M., & Mestre, O. (2013). Clustering of maxima: Spatial dependencies among heavy rainfall in France. *Journal of Climate*, *26*(20), 7929–7937.
- Bin, O., & Polasky, S. (2004). Effects of flood hazards on property values: Evidence before and after Hurricane Floyd. *Land Economics*, *80*(4), 490–500.
- Bonnin, G. M., Martin, D., Lin, B., Parzybok, T., Yekta, M., & Riley, D. (2006). Precipitation-frequency atlas of the United States. *NOAA Atlas*, *14*(2), 1–65.
- Carreau, J., Naveau, P., & Neppel, L. (2016). Characterization of homogeneous regions for regional peaks-over-threshold modeling of heavy precipitation. Retrieved from <http://hal.ird.fr/ird-01331374> (working paper or preprint).
- Crichton, D. (2008). Role of insurance in reducing flood risk. *The Geneva Papers on Risk and Insurance-Issues and Practice*, *33*(1), 117–132.
- FEMA (2015). Flooding our nations most frequent and costly natural disaster. *Fact Sheet* (p. 2, 10). Retrieved from <https://www.fbiic.gov/public/2010/mar/FloodingHistoryandCausesFS.PDF>
- Fischer, E. M., Beyerle, U., & Knutti, R. (2013). Robust spatially aggregated projections of climate extremes. *Nature Climate Change*, *3*(12), 1033–1038.
- Fischer, E. M., & Knutti, R. (2014). Detection of spatially aggregated changes in temperature and precipitation extremes. *Geophysical Research Letters*, *41*, 547–554. <https://doi.org/10.1002/2013GL058499>
- Gleckler, P. J., Santer, B. D., Domingues, C. M., Pierce, D. W., Barnett, T. P., Church, J. A., et al. (2012). Human-induced global ocean warming on multidecadal timescales. *Nature Climate Change*, *2*(7), 524–529.
- Gong, X., & Richman, M. B. (1995). On the application of cluster analysis to growing season precipitation data in North America east of the Rockies. *Journal of Climate*, *8*(4), 897–931.
- Hargrove, W. W., & Luxmoore, R. J. (1998). A new high-resolution national map of vegetation ecoregions produced empirically using multivariate spatial clustering. Retrieved from <http://www.esd.ornl.gov/~hnw/esri98>
- Herger, N., Abramowitz, G., Knutti, R., Angéllil, O., Lehmann, K., & Sanderson, B. M. (2017). Selecting a climate model subset to optimise key ensemble properties. *Earth System Dynamics Discussions*, *9*, 135–151. <https://doi.org/10.5194/esd-2017-28>, in review.
- Herring, S. C., Hoerling, M. P., Kossin, J. P., Peterson, T. C., & Stott, P. A. (2015). Explaining extreme events of 2014 from a climate perspective. *Bulletin of the American Meteorological Society*, *96*(12), S1–S172.
- Kay, J. E., Deser, C., Phillips, A., Mai, A., Hannay, C., Strand, G., et al. (2015). The Community Earth System Model (CESM) large ensemble project: A community resource for studying climate change in the presence of internal climate variability. *Bulletin of the American Meteorological Society*, *96*(8), 1333–1349.
- Kennel, C. F., Briggs, S., & Victor, D. G. (2016). Making climate science more relevant. *Science*, *354*(6311), 421–422.
- King, D., Schrag, D., Dadi, Z., Ye, Q., & Ghosh, A. (2015). Climate change: A risk assessment. Centre for Policy Research, University of Cambridge. Retrieved from <http://www.csap.cam.ac.uk/media/uploads/files/1/climate-change-a-risk-assessment-v9-spreads.pdf>, Accessed, 12.
- Knutti, R., Abramowitz, G., Collins, M., Eyring, V., Gleckler, P. J., Hewitson, B., et al. (2010). Good practice guidance paper on assessing and combining multi model climate projections. In *IPCC Expert Meeting on Assessing and Combining Multimodel Climate Projections* (pp. 1).
- Kundzewicz, Z. W., & Takeuchi, K. (1999). Flood protection and management: Quo vadimus? *Hydrological Sciences Journal*, *44*(3), 417–432.
- Kunkel, K. E., Andsager, K., & Easterling, D. R. (1999). Long-term trends in extreme precipitation events over the conterminous United States and Canada. *Journal of Climate*, *12*(8), 2515–2527.
- Kunkel, K. E., Easterling, D. R., Redmond, K., & Hubbard, K. (2003). Temporal variations of extreme precipitation events in the United States: 1895–2000. *Geophysical Research Letters*, *30*(17), 1900. <https://doi.org/10.1029/2003GL018052>
- Kunreuther, H., Heal, G., Allen, M., Edenhofer, O., Field, C. B., & Yohe, G. (2013). Risk management and climate change. *Nature Climate Change*, *3*(5), 447.
- Liscum, F., & East, J. W. (1995). Floods in southeast Texas, October 1994 (Tech. Rep.). Reston: US Geological Survey.
- Maxwell, K., Grambsch, A., Kosmal, A., Larson, L., & Sonti, N. (2018). Built environment, urban systems, and cities. In D. R. Reidmiller, et al. (Eds.), *2018. Impacts, risks, and adaptation in the United States: Fourth national climate assessment, volume II* (Vol. 2, pp. 438–478). Washington, DC: US Global Change Research Program.

- Min, S.-K., Zhang, X., Zwiers, F. W., & Hegerl, G. C. (2011). Human contribution to more-intense precipitation extremes. *Nature*, *470*(7334), 378–381.
- Mishra, A. K., & Singh, V. P. (2010). Changes in extreme precipitation in Texas. *Journal of Geophysical Research*, *115*, D14106. <https://doi.org/10.1029/2009JD013398>
- Morice, C. P., Kennedy, J. J., Rayner, N. A., & Jones, P. D. (2012). Quantifying uncertainties in global and regional temperature change using an ensemble of observational estimates: The HadCRUT4 data set. *Journal of Geophysical Research*, *117*, D08101. <https://doi.org/10.1029/2011JD017187>
- Munich, R. E. (2015). *Natcatservice loss events worldwide 1980–2014*. Munich: Munich Reinsurance. Retrieved from <https://reliefweb.int/report/world/natcatservice-loss-events-worldwide-1980-2015>
- National Academies of Sciences, Engineering, and Medicine (2016). *Characterizing Risk in Climate Change Assessments: Proceedings of a Workshop*. Washington, DC: The National Academies Press. <https://doi.org/10.17226/23569>
- National Park Service news release, October 10, 2006 (n.d.). Retrieved from <https://www.nps.gov/arch/learn/news/news101006.htm>, (Accessed: 2018-03-21).
- Pendergrass, A. G., Lehner, F., Sanderson, B. M., & Xu, Y. (2015). Does extreme precipitation intensity depend on the emissions scenario? *Geophysical Research Letters*, *42*, 8767–8774. <https://doi.org/10.1002/2015GL065854>
- Pielke, R. A. Jr., & Downton, M. W. (2000). Precipitation and damaging floods: Trends in the United States, 1932–97. *Journal of Climate*, *13*(20), 3625–3637.
- Rappaport, E. N. (2000). Loss of life in the United States associated with recent Atlantic tropical cyclones. *Bulletin of the American Meteorological Society*, *81*(9), 2065–2073.
- Riahi, K., Rao, S., Krey, V., Cho, C., Chirkov, V., Fischer, G., et al. (2011). RCP 8.5—A scenario of comparatively high greenhouse gas emissions. *Climatic Change*, *109*(1-2), 33.
- Sanderson, B. M., Wehner, M., & Knutti, R. (2017). Skill and independence weighting for multi-model assessments. *Geoscientific Model Development*, *10*(6), 2379.
- Singh, M. S., & O’Gorman, P. A. (2014). Influence of microphysics on the scaling of precipitation extremes with temperature. *Geophysical Research Letters*, *41*, 6037–6044. <https://doi.org/10.1002/2014GL061222>
- Singh, A., Yadav, A., & Rana, A. (2013). K-means with three different distance metrics. *International Journal of Computer Applications*, *67*(10), 13–17.
- Stern, N. (2013). The structure of economic modeling of the potential impacts of climate change: Grafting gross underestimation of risk onto already narrow science models. *Journal of Economic Literature*, *51*(3), 838–59.
- Taylor, K. E., Stouffer, R. J., & Meehl, G. A. (2012). An overview of CMIP5 and the experiment design. *Bulletin of the American Meteorological Society*, *93*(4), 485–498.
- Tollan, A. (2002). Land-use change and floods: What do we need most, research or management? *Water Science and Technology*, *45*(8), 183–190.
- Trenberth, K. E., Dai, A., Rasmussen, R. M., & Parsons, D. B. (2003). The changing character of precipitation. *Bulletin of the American Meteorological Society*, *84*(9), 1205–1217.
- Wahlstrom, M., & Guha-Sapir, D. (2015). *The human cost of weather-related disasters 1995–2015*. Geneva: United Nations International Strategy for Disaster Reduction.
- Weaver, C. P., Moss, R. H., Ebi, K. L., Gleick, P. H., Stern, P. C., Tebaldi, C., et al. (2017). Reframing climate change assessments around risk: Recommendations for the US National Climate Assessment. *Environmental Research Letters*, *12*(8), 080201.
- Wobus, C., Gutmann, E., Jones, R., Rissing, M., Mizukami, N., Lorie, M., et al. (2017). Climate change impacts on flood risk and asset damages within mapped 100-year floodplains of the contiguous United States. *Natural Hazards and Earth System Sciences*, *17*(12), 2199.
- Wuebbles, D. J., Fahey, D. W., Hibbard, K. A., Dokken, D. J., Stewart, B. C., & Maycock, T. K. (2017). *Climate science special report: Fourth national climate assessment*. Washington, DC: US Global Change Research Program.
- Wuebbles, D., Meehl, G., Hayhoe, K., Karl, T. R., Kunkel, K., Santer, B., et al. (2014). CMIP5 climate model analyses: Climate extremes in the United States. *Bulletin of the American Meteorological Society*, *95*(4), 571–83.
- Yavuz, H., & Erdoğan, S. (2012). Spatial analysis of monthly and annual precipitation trends in Turkey. *Water Resources Management*, *26*(3), 609–621.
- Zhang, X., Hogg, W. D., & Mekis, É. (2001). Spatial and temporal characteristics of heavy precipitation events over Canada. *Journal of Climate*, *14*(9), 1923–1936.